Modeling of Inhomogeneous Intensity Distribution of X-Ray Source in Radiographic Images

Ayhan Yüksel, Zümray Dokur, Mehmet Korürek, Tamer Ölmez
Department of Electronics and Communication Engineering, Istanbul Technical University, 34469 Maslak, Istanbul, Turkey
{yukselay, dokur, korurek, olmezt}@itu.edu.tr

***Abstract*- X-ray bone images are used in the areas such as bone age assessment, bone mass assessment and examination of bone fractures. The computer aided analysis leads to operator independent, subjective and fast results.**

In this study, inhomogeneous intensity distribution of X-ray source is eliminated from hand radiographic images. This distribution of X-ray source is modeled by two methods: i) Heel effect, and ii) near field effect. Two models are comparatively examined to represent intensity distribution of X-ray source. The parameter of first and second model is estimated by using simplex method and genetic algorithms respectively. Inhomogeneous intensity distribution of X-ray source is corrected for all image pixels retrospectively.

Variance values of pixels in the background are computed to test the two methods. It is observed that variance value of pixels in background decreases more by the novel method compared to the other method.

***Index Terms*- X-Ray Hand image Analysis, Genetic Algorithms, Image Restoration, Image Enhancements.**

I. INTRODUCTION

X-ray bone images are used in the areas such as bone age assessment [1-5], bone mass assessment [6, 7] and examination of bone fractures [8]. Extraction of bone tissue from other tissues and background (segmentation) is one of the main steps in such applications. Segmentation of medical images is a challenging problem and a necessary first step in many image analysis and classification processes [8].

In the analysis of 2D hand X-ray images, there are some specific problems [9]. In addition to these problems, X-ray beams do not touch to the examined material at equal strength due to the X-ray beam source location. As a result, inhomogeneous intensity distribution occurs on the resulted X-ray image.

Behiels et al. studied inhomogeneous intensity distribution correction, which caused intensity uniformity along anode cathode axes due to small anode angle allowing the use of a large focal spot [10]

In this study, a novel model for simulation of inhomogeneous intensity distribution of X-ray source in radiographic hand images was proposed. In novel model, parameters were estimated using genetic algorithms. Intensity distribution becomes homogenous by the help of the implemented intensity adjustment algorithm.

II. METHOD

Two models are comparatively examined to represent intensity distribution of X-ray source: i) heel effect, and ii) near field effect.

A. Heel Effect

Cathode is the source of electron in an x-ray tube. X-ray photons are created when accelerated electrons hit target anode in a high voltage electrical field. Anode is inclined by a small angle θ so that smaller focal spot is obtained for better image quality as shown in Fig. 1. The inclination in anode disk causes X-ray photons to leave the anode with different intensities. It can be assumed that x-ray photons are created by a point source which stands in a small distance beneath the surface of the anode. Therefore, when the X-ray photons are transmitting through the anode material, photons which are closer to cathode side pass shorter distance in anode disk than that are close to anode side. This occurrence creates a non-uniform X-ray intensity seen on radiographic images and is called as Heel Effect. Heel effect creates a non-uniform intensity over anode cathode axis.

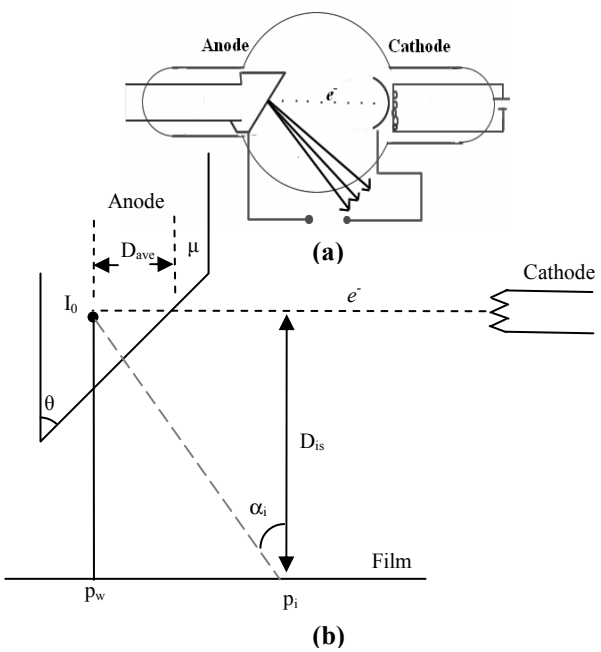

Fig. 2. (a) A classical X-ray tube. (b) A schematic for anode heel effect

978-1-4244-2881-6/08/$25.00 ©2008 IEEE

Mathematical model for Heel effect can be derived from Fig. 1b. Where, I_0 is the intensity of point source, θ is anode's inclination angle, D_{ave} is an average depth that electrons travel inside the anode, D_{is} is the height of point source according to optical film, μ is the X-ray linear attenuation coefficient of anode material, p_w is the projection of point source on anode-cathode axis and p_i is the projection of any point on to this axis. As seen on figure h1, incident intensity of X-ray photon varies with its projected position on anode-cathode axis, p_i. According to Fig. 1b, incident X-ray photon intensity I_i at any position (x_i, y_i) is given by (1):

$$I_i = I_M - I_0 \cdot e^{-\mu \cdot D_{ave} \cdot \frac{\sqrt{1+(\frac{p_i - p_w}{D_{is}})^2}}{\tan\theta + \frac{p_i - p_w}{D_{is}}}} \quad (1)$$

According to (1), five parameters; I_0, p_w, $\tan\theta$, D_{is}, $uD_{ave.}$ are needed to be estimated. For this purpose, pixels that belong to background, where no attenuation due to tissues exists, were sampled. Then, the best parameters that calculate the sampled pixel intensities with minimum error were searched by Simplex method [10].

Before estimation of parameters, anode-cathode axis was determined. Randomly selected samples from background were sorted in increasing order according to their intensity values. Sorted pixels were separated into two sets from half; pixels with lower intensities and pixels with higher intensities. Than, middle points of the two sets were calculated by taking average of $-x$ and $-y$ coordinate values separately. Anode-Cathode axis direction was determined by the vector that is from one middle point to another. It was observed that, the same direction is obtained every time when the method is repeated. Then, sampled points' projections onto anode-cathode axis were calculated according to a selected reference point.

B. A Novel Model

In this study, X-ray source was modeled as a near field point source with intensity parameter Io and position parameters x_0, y_0, z_0. Non-uniform intensity distribution is difficult to observe on hand region due to different absorption characteristics of tissues. For this purpose, background area where there is no absorption attenuation exists was sampled from the image automatically. In finding the best position and intensity parameter set, genetic algorithms were used because of their robust structure in optimization problems [11]. After calculation of the model parameters, an intensity correction procedure was implemented in whole image in order to create uniformly distributed intensity profile. In Fig. 1, main steps of the intensity correction process are depicted.

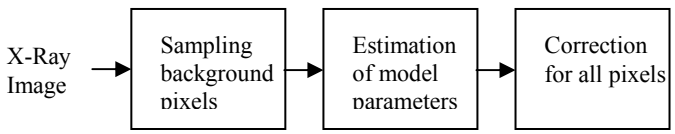

Fig. 1 Main steps of the intensity correction process

1) Near Field Point Source: X-ray photon with intensity Io that departs from a point source causes blackening on optical film by the following formula [12]:

$$I_i = I_M - I_o e^{-\int \mu_z dz} \cos(\theta_i) \quad (1)$$

In the Equ. 1, I_i is the perpendicular component of X-ray intensity vector at position (x_i, y_i), I_M is a position independent constant to obtain negative image, θ_i is the angle of incident photon at (x_i, y_i) according to the normal of image plane, $\int \mu_z dz$ is the total absorption of medium where X-ray traverses. A three dimensional representation of the model is shown in Fig. 2. Here, $\cos(\theta_i)$ can be formulated by the following equation in 3-D space,

$$\cos(\theta_i) = h_0 / \sqrt{d_i^2 + h_0^2} \qquad d_i = \sqrt{(x_i - x_0)^2 + (y_i - y_0)^2} \quad (2)$$

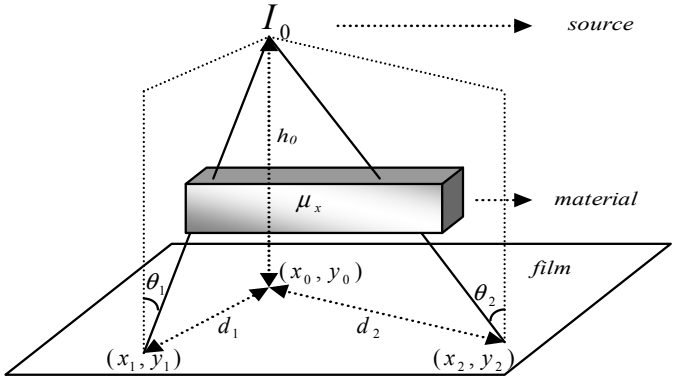

Fig. 2. 3-D representation of the model of X-ray Source

where d_i is the Euclidean distance between projection position of X-ray source on film (x_0, y_0) and position (x_i, y_i); h_0 is the elevation of X-ray source with respect to film.

According to the proposed model, when an X-ray photon arrives at a background pixel, no attenuation exists and exponential term in the Equ. 1 can be omitted. Hence, for a background pixel, intensity is calculated by the following equation:

$$I_i = I_M - I_o \cos(\theta_i) \quad (3)$$

In the Equ. 3, it is evident that the intensity over background will vary according to the position or the distance to the projection of X-ray source. This estimation implies ring shaped intensity distribution profile at the background where each ring corresponds to the same intensity. These rings can be noticed on the image by displaying different segments of the histogram. In Fig. 3, different rings special to the selected histogram intervals can be viewed obviously.

2) Estimating Model Parameters by Using Genetic Algorithms: Each genetic string in the pool represents four parameters in the Equ. 3: i) x position (x_0), ii) y position (y_0), iii) height of X-ray source (h_0) and iv) maximum intensity value of X-ray image (I_M). Each parameter is represented in decimal format.

The fitness function used in genetic algorithm was designed in order to minimize the background pixel intensity variance. According to the proposed model, a background pixel intensity value is calculated as given in the Equ. 3. In this equation, for the given estimated parameters $\hat{x}_0, \hat{y}_0, \hat{h}_0, \hat{I}_M$; an estimation of X-ray source intensity $\hat{I}_0$ is found by the following equation:

$$\hat{I}_0 = (\hat{I}_M - I_i)/\cos\theta_i \qquad (4)$$

$$\cos\theta_i = \hat{h}_0 / \sqrt{\hat{h}_0 + (x_i - \hat{x}_0)^2 + (y_i - \hat{y}_0)^2}$$

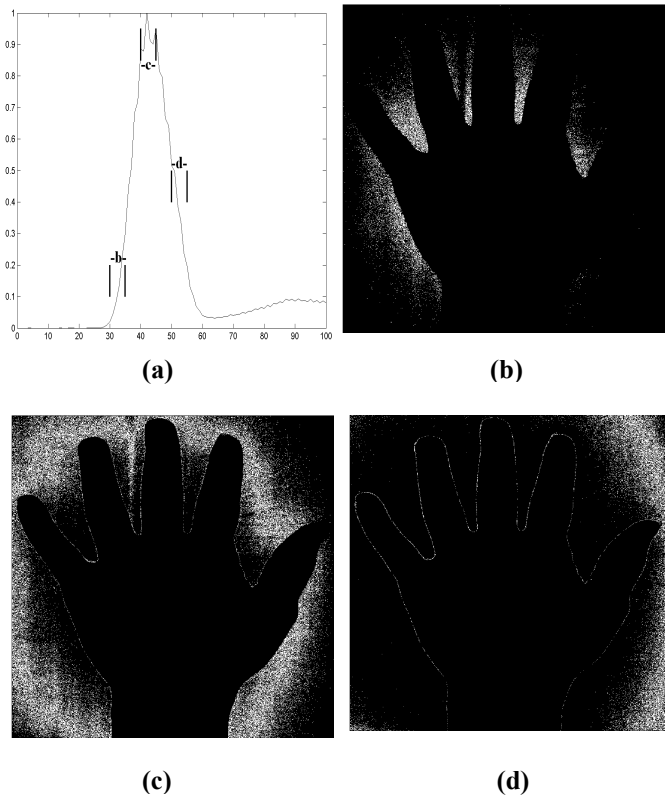

(a) **(b)**

(c) **(d)**

Fig. 3. Rings special to the selected histogram intervals

By combining the (3) and (4), estimated X-ray source intensity can be calculated as given in the (5):

$$\hat{I}_0 = \frac{(\hat{I}_M - I_i)}{\cos\hat{\theta}_i} = \frac{(\hat{I}_M - I_M)}{\cos\hat{\theta}_i} + I_0 \frac{\cos\theta_i}{\cos\hat{\theta}_i} \qquad (5)$$

The Equ. 5 is calculated for all background samples and a set of $\hat{I}_0$ values is obtained. When model parameters are estimated perfectly, each $\hat{I}_0$ will be equal to I_0 . Therefore, the error function to be minimized can be considered as the variance of $\hat{I}_0$ values for each sampled point positions (x, y) at background as given in the Equ. 6.

$$E = \mathrm{var}(\hat{I}_0) \qquad F_{Fitness} = 1/(1+E) \qquad (6)$$

Genetic algorithm will execute selection, reproduction and mutation processes iteratively in order to find the most suitable parameters which are maximized the fitness function. When the parameters are calculated with minimum error, it is possible to know I_0 by the mean of the $\hat{I}_0$ values.

3) Correction of non-uniform intensity distribution: Corrected image pixel value can be obtained by the following formula;

$$Ic_i = \hat{I}_M - (\hat{I}_M - I_i)/DE$$

$$DE = \quad for\ the\ first\ \mathrm{model}$$

$$DE = \cos\hat{\theta}_i \quad for\ the\ second\ \mathrm{model} \qquad (7)$$

In (7), Ic_i represents the corrected image pixel at position (*x, y*). These formulas are applied to all image pixels. As it can be easily noticed. 3-D representation of background pixels for the original and the corrected images by two methods are shown in Fig. 4.

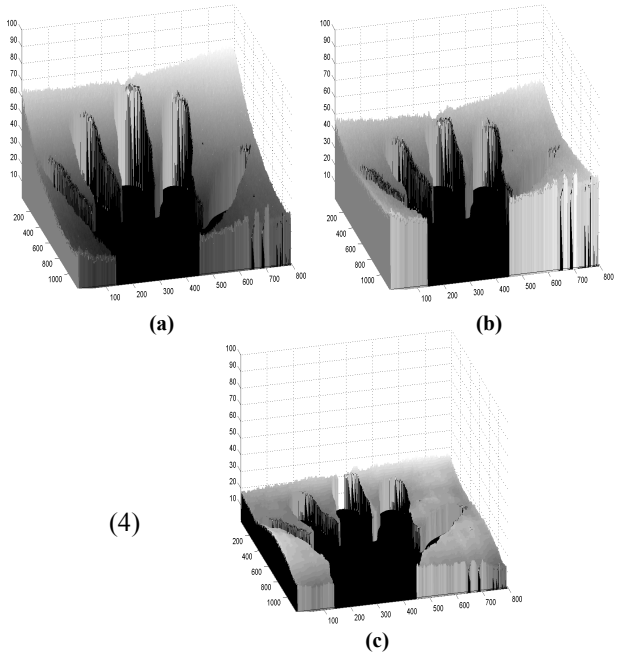

(a) **(b)**

(4)

(c)

Fig. 4. 3-D representation of (a) the original image, (b) the corrected image first method (c) the corrected image proposed method

III. COMPUTER SIMULATION RESULTS

Hand radiographic images used in the study were acquired from South California University Image Processing Laboratory Database [13]. All methods and algorithms are realized with MATLAB 7.1 ® in a 1.73 GHz Intel Centrino Laptop.

Hand X-ray images were used for intensity correction procedure. Obtained results were illustrated on a sample image (image name:4524) in the database. In the Fig. 5, original image and *x, y* coordinates of X-ray source are shown. For this radiograph, model parameters were found by the genetic algorithms as follows; x_o=303, y_o=870, h_o=1134, I_M =255.

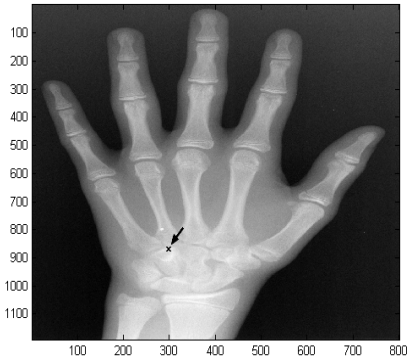

Fig. 5 Original X-Ray image and estimated position of source on X-ray film

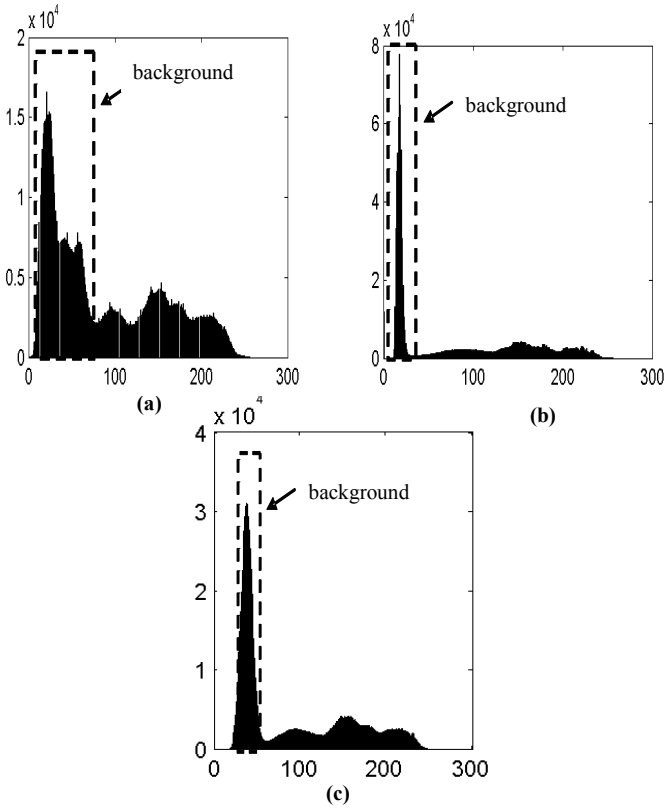

Fig. 6. 3-D representation of (a) the original image, (b) the corrected image first method (c) the corrected image proposed method

Performance of proposed algorithm was analyzed by calculating the intensity variance of background pixels in original image and corrected image. Background gray level histograms will show the effect of correction algorithm. Histograms of the original and the corrected images are given in Fig. 6.a, 6.b and 6.c respectively. Histograms in the Fig. 6 is formed by using results in Fig 4. As seen in the histograms, methods cause background pixels to have smaller variance values. Performance results for all images are given in Table 1.

IV. CONCLUSION

In this study, it is observed that proposed model more represents the inhomogeneous intensity distribution of X-ray point source than other model and, the parameters of proposed model is easily determined by the genetic algorithms.

In this study, we made a special effort not to loss the originality of the hand radiographic images. The originality of them is important to determine the age of bone or to measure the bone densities.

In feature study, the effect of modeling inhomogeneous intensity distribution of X-ray source on the segmentation results of hand and bone tissues will be investigated. And also, the effect of noise in finding the parameters of novel model by genetic algorithms will be analyzed.

REFERENCES

[1] Garcia, R.L., Fernandez, M.M., Arribas, J.I. and Lopez C.A. (2003). A fully automatic algorithm for contour detection of bones in hand radiographs using active contours, *Int. Conf. on Ima. Pro.*, 421-424.

[2] Han, C.C., Lee, C.H. and Peng, W.L. (2007). Hand radiograph image segmentation using a coarse-to-fine strategy, *Pattern Recognition,* 40, 2994-3004.

[3] Zhang, A., Gertych, A. and Liu, B.J. (2007). Automatic bone age assessment for young children from newborn to 7-year-old using carpal bones, *Computerized Medical Imaging and Graphics,* 31, 299-310.

[4] Mahmoodi S., Sharif B.S., Chester, E.G., Owen J.P. and Lee R. (2000). Skeletal growth estimation using radiographic image processing and analysis, *IEEE Tran. on Inf. Tech. in Bio.* , 4, 292-297.

[5] Pietka, E., Kurkowska, S.P., Gertych A. and Cao, F. (2003). Integration of computer assisted bone age assessment with clinical PACS, *Computerized Medical Imaging and Graphics,* 27, 217-228.

[6] Sotoca, J.M., Inesta, J.M. and Belmonte M.A. (2003). Hand bone segmentation in radioabsorptiometry images for computerised bone mass assessment, *Computerized Medical Imaging and Graphics,* 27, 459-467.

[7] Haidekker, M.A., Stevens, H.Y. and Frangos J.A. (2004). Computerised methods for X-ray-based small bone densitometry, *Computer Methods and Programs in Biomedicine,* 73, 35-42.

[8] Jiang, Y. and Babyn, P. **(**2004). X-ray bone fracture segmentation by incorporating global shape model priors into geodesic active contours, *Computer Assisted Radiology and Surgery*, 219-224.

[9] Ogiela, M. R., Tadeusiewicz, R. and Ogiela L. (2006). Graph image language techniques supporting radiological, hand image interpretations, Computer Vision and Image Understanding 103, 112–120.

[10]Behils G., Maes F., Vandermeulen D., Suetens P. (2002). Retrospective Correction of the hell effect in hand radiographs, Medical Image Analysis, 6, 183-190.

[11]Chan, Z.S.H., Kasabov, N. (2004). Gene trajectory clustering with a hybrid genetic algorithm and expectation maximization method, Proceedings of IEEE Int. Jo. Con. on Neural Networks, 3, 1669- 1674.

[12]Guy C. and Ffytche D. (2000). An Introduction to the Principles of Medical Imaging. Imperial College Press, London**.**

[13] http://www.ipilab.org/

TABLE I

PERFORMANCES FOR ORIGINAL AND CORRECTED IMAGES BY FIRST AND PROPOSED METHODS

Image Name [13]	**3229**	**3842**	**4335**	**4482**	**4494**	**4524**	**5104**	**5209**	**5268**	**5365**
Background pixel variances of original images	**41.8**	**80.4**	**58.5**	**17.6**	**49**	**74.2**	**41.7**	**82.7**	**60.8**	**63.2**
Background pixel variances after first method	**15**	**10.5**	**6.5**	**10.8**	**15.2**	**21.0**	**19.8**	**17.4**	**13.1**	**18.6**
Background pixel variances after proposed method	**8.2**	**5.3**	**8.3**	**6.9**	**7.3**	**5.7**	**7.3**	**11.5**	**3.7**	**11**